ONERA

Ecole Polytechnique Fédérale de Lausanne , Suisse

22 Novembre 2007

Second order closure turbulence modeling: from Reynolds stress models to large eddy simulations

Bruno CHAOUAT, ONERA, Palaiseau, France

OUTLINE

- Presentation of ONERA, French agencie for aeronautics and space
- Turbulence modeling from RANS (Reynolds Averaged Navier-Stokes) to LES (Large eddy Simulation)
- Second order closure modeling, Reynolds Stress Model (RSM)
- Numerical method
- RSM modeling of internal and external flows encountered in aeronautics
- Mathematical physics formalism that allows transposition from RANS to LES models
  - General PITM formalism (Schiestel and Dejoan, 2005, Chaouat and Schiestel, 2005)
  - Turbulent energy subfilter model based on the transport equations for k_{sgs} and ϵ_{sgs}
  - Turbulent stress subfilter model based on the transport equations for $(\tau_{ij})_{sgs}$ and ϵ_{sgs}
- Hybrid RANS/LES simulations of homogeneous and non-homogeneous turbulent flows

ONERA, FRENCH AGENCIE FOR AERONAUTICS AND SPACE

- Manpower and facilities (permanent personnel of over 2000)
  - Paris area : headquarter, computer center and research laboratories
  - Modane and Le Fauga-Mauzac : industrial wind tunnels and test facilities for propulsion
  - Toulouse and Lille: research laboratories
- Statut, mission and activities
  - Scientific and technical government establishment
  - Develops and orients research in the aerospace field
  - Makes results available to industry
  - Field: Fluid mechanics and energetics, Material and structures, Physics, Information processing and systems, Engineering and testing facilities

ONERA

FROM RANS TO LES MODELING

- RANS modeling : many contributions in the past forty years (Launder, Lumley, Gatski et al.)
  - First order closure (Launder, 1972, Menter, 1990)
  - Second order closure (Launder, Lumley, Gatski et al. 1975-2007)
- Academic large eddy simulation
  - Smagorinsky model (1963)
  - Dynamic subgrid-scale model (Piomelli and Germano, 1991)
  - Structure-function model (Lesieur, 1996) etc ....
- Hybrid zonal approach
  - Detached-Eddy simulation DES (Spalart-Almaras, 1994)
- Hybrid continuous approach
  - Subgrid PITM model for $(\tau_{ij})_{sgs}$ and ϵ_{sgs}, (Chaouat and Schiestel, 2005)
  - Subgrid PANS model for k_{sgs} and ϵ_{sgs}, (Girimaji, 2006)

ONERA

SECOND ORDER CLOSURE

- **Transport equation for the statistical velocity** $\langle u_i \rangle$ **RANS approach**

$$\frac{\partial \langle u_i \rangle}{\partial t} + \frac{\partial}{\partial x_j}\Big(\langle u_i \rangle \langle u_j \rangle \Big) = -\frac{1}{\rho}\frac{\partial \langle p \rangle}{\partial x_i} + \nu \frac{\partial^2 \langle u_i \rangle}{\partial x_j \partial x_j} - \frac{\partial \tau_{ij}}{\partial x_j} \qquad \textbf{(1)}$$

with $\tau_{ij} = \langle u_i u_j \rangle - \langle u_i \rangle \langle u_j \rangle$

- **Transport equation for the filtered velocity** $\bar{u}_i$ **LES and continuous HYBRID approaches**

$$\frac{\partial \bar{u}_i}{\partial t} + \frac{\partial}{\partial x_j}(\bar{u}_i \bar{u}_j) = -\frac{1}{\rho}\frac{\partial \bar{p}}{\partial x_i} + \nu \frac{\partial^2 \bar{u}_i}{\partial x_j \partial x_j} - \frac{\partial (\tau_{ij})_{sgs}}{\partial x_j} \qquad \textbf{(2)}$$

with $(\tau_{ij})_{sgs} = \overline{u_i u_j} - \bar{u}_i \bar{u}_j$

- **Second order closure is based on the transport equation of the tensor** τ_{ij} **or** $(\tau_{ij})_{sgs}$

REYNOLDS STRESS MODEL FORMULATION

- **Exact transport equation for the Reynolds stress tensor τ_{ij}**

$$\frac{\partial \tau_{ij}}{\partial t} + \langle u_k \rangle \frac{\partial \tau_{ij}}{\partial x_k} = P_{ij} - 2\Omega_p \left(\epsilon_{jpk}\tau_{ki} + \epsilon_{ipk}\tau_{kj} \right) + \Phi_{ij} - \epsilon_{ij} + J_{ij} \qquad \text{(3)}$$

  - **Production term P_{ij} :**

$$P_{ij} = -\tau_{ik}\frac{\partial \langle u_j \rangle}{\partial x_k} - \tau_{jk}\frac{\partial \langle u_i \rangle}{\partial x_k} \qquad \text{(4)}$$

  - **Coriolis force :** $2\Omega_p \left(\epsilon_{jpk}\tau_{ki} + \epsilon_{ipk}\tau_{kj} \right)$
  - **Pressure-strain rate correlation Φ_{ij} :**

$$\Phi_{ij} = \left\langle \frac{p'}{\rho} \left(\frac{\partial u'_i}{\partial x_j} + \frac{\partial u'_j}{\partial x_i} \right) \right\rangle \qquad \text{(5)}$$

  - **Disssipation rate tensor ϵ_{ij} :**

$$\epsilon_{ij} = 2\nu \left\langle \left(\frac{\partial u'_i}{\partial x_k} \frac{\partial u'_j}{\partial x_k} \right) \right\rangle \qquad \text{(6)}$$

  - **Laminar and turbulent diffusion processes J_{ij} :**

$$J_{ij} = \nu \frac{\partial^2 \tau_{ij}}{\partial x_k \partial x_k} - \frac{\partial}{\partial x_k} \left\langle (u'_i u'_j u'_k) \right\rangle - \frac{1}{\rho}\frac{\partial}{\partial x_k} \left(\langle p' u'_i \rangle \ \delta_{jk} + \langle p' u'_j \rangle \ \delta_{ik} \right) \qquad \text{(7)}$$

REYNOLDS STRESS MODEL

- **Modeling of the redistribution term Φ_{ij} based on the fluctuating pressure equation**

$$\frac{1}{\rho}\frac{\partial^2 p'}{\partial x_i \partial x_i} = -2\left(\frac{\partial \langle u_i \rangle}{\partial x_j} + \epsilon_{ikj}\Omega_k\right)\frac{\partial u'_j}{\partial x_i} - \frac{\partial^2}{\partial x_j \partial x_i}\left(u'_i u'_j - \langle u'_i u'_j \rangle\right) \quad \textbf{(8)}$$

$$=> \Phi_{ij} = \Phi^1_{ij} + \Phi^2_{ij} + \Phi^w_{ij} \quad \textbf{(9)}$$

  - **Action of turbulence on itself Φ^1_{ij}**
  - **Action of mean velocity gradient Φ^2_{ij}**

$$2)\ \Phi^2_{ij} = M_{ijkl}\left(\frac{\partial \langle u_k \rangle}{\partial x_l} + \epsilon_{kpl}\Omega_p\right) \quad \textbf{(10)}$$

$$M_{ijkl} = \frac{1}{2\pi}\iiint_\Omega \left\langle \frac{\partial u'^*_l}{\partial x^*_k}\left(\frac{\partial u'_i}{\partial x_j} + \frac{\partial u'_j}{\partial x_i}\right)\right\rangle \frac{1}{|r - r^*|}\, d^3 r^* \quad \textbf{(11)}$$

  - **Wall reflexion of the pressure fluctuations Φ^w_{ij}**

FINAL REYNOLDS STRESS MODELED

- **Modeling of the Reynolds stress model for low Reynolds number using the invariant anisotropy tensor (Launder and Shima, 1989)**

$$\frac{\partial \tau_{ij}}{\partial t} + \langle u_k \rangle \frac{\partial \tau_{ij}}{\partial x_k} = P_{ij} - 2\Omega_p \left(\epsilon_{jpk}\tau_{ki} + \epsilon_{ipk}\tau_{kj}\right) - \frac{2}{3}\epsilon + J_{ij}$$
$$-c_1(A)\frac{\epsilon}{k}\left(\tau_{ij} - \frac{2}{3}k\delta_{ij}\right) - c_2(A)\left(P_{ij} + \frac{1}{2}P^R_{ij} - \frac{1}{3}P_{mm}\delta_{ij}\right) + \Phi^w_{ij} \quad \textbf{(12)}$$

- **Modeling of the dissipation-rate equation (Launder and Shima, 1989; Chaouat, 2001)**

$$\frac{\partial \epsilon}{\partial t} + \langle u_j \rangle \frac{\partial \epsilon}{\partial x_j} = -c_{\epsilon_1}\frac{\epsilon}{k}\tau_{ij}\frac{\partial \langle u_j \rangle}{\partial x_i} - c_{\epsilon_2}\frac{\tilde{\epsilon}\epsilon}{k} + J_\epsilon + E_\epsilon \quad \textbf{(13)}$$

where

$$E_\epsilon = c_{\epsilon_3}\,\nu\frac{k}{\epsilon}\tau_{kl}\frac{\partial^2 \langle u_i \rangle}{\partial x_k \partial x_j}\frac{\partial^2 \langle u_i \rangle}{\partial x_l \partial x_j} \quad \textbf{(14)}$$

$c_{\epsilon_1} = 1.45$, $c_{\epsilon_2} = 1.9$, $c_{\epsilon_3} = 0.1$, $c_\epsilon = 0.18$ **and** $\tilde{\epsilon} = \epsilon - 2\nu(\partial\sqrt{k}/\partial x_n)^2$.

REALIZABILITY CONDITIONS

- **RSM Models have been developed upon basic physical considerations**
- **Realizability conditions: positive values of the principal invariants I_i that appear in the characteristic polynomial $P(\lambda) = \lambda^3 - I_1\lambda^2 + I_2\lambda - I_3$ of the matrix formed by the components τ_{ij} (Schumann, 1977)**
- **Week form of the realizability conditions: $\partial\tau_{\alpha\alpha}/\partial t > 0$ when $\tau_{\alpha\alpha}$ goes to zero (Speziale et al., 1994)**
  - **Transport equation of the turbulent stress component $\tau_{\alpha\alpha}$ in the prinicipal axes can be written (summation on β)**

$$\frac{\partial\tau_{\alpha\alpha}}{\partial t} + \langle u_\beta\rangle \frac{\partial\tau_{\alpha\alpha}}{\partial x_\beta} = P_{\alpha\alpha} + P^R_{\alpha\alpha} - \frac{2}{3}\epsilon - c_1\frac{\epsilon}{k}(\tau_{\alpha\alpha} - \tfrac{2}{3}k)$$
$$-c_2(P_{\alpha\alpha} + \tfrac{1}{2}P^R_{\alpha\alpha} - \tfrac{1}{3}P_{\beta\beta}) \quad \textbf{(15)}$$

  - **Condition to satisfy: (Chaouat, 2001)**

$$\boxed{c_1(A) \geq 1 - c_2\frac{P_{\beta\beta}}{2\epsilon}} \quad \textbf{(16)}$$

where $A = 1 - 9/8(A_2 - A_3)$ and $A_2 = a_{ij}a_{ji}$, $A_3 = a_{ij}a_{jk}a_{ki}$.

NUMERICAL METHOD

- Three-dimensional compressible code for solving the energy or the stress model
  - $\rho, u_1, u_2, u_3, E, k, \epsilon$
  - $\rho, u_1, u_2, u_3, E, \tau_{11}, \tau_{12}, \tau_{13}, \tau_{22}, \tau_{23}, \tau_{33}, \epsilon$
- Finite volumes technique: fluxes conservative method

$$\frac{\partial U}{\partial t} = -\frac{1}{v(\Omega)} \sum_{\sigma} (F_k - F_{v\,k}) n_{k\sigma} A_\sigma + S \tag{17}$$

- Fourth order Runge-Kutta scheme in time discretization
- Implicit scheme in time for the treatment of the turbulent equations
- Second order centered scheme in space discretization (MUSCL scheme)
- CPU time : the stress model (12 transport equations) only requires 25 % more time than the energy model (7 transport equations)

NUMERICAL METHOD

- **Spatial discretization scheme**
  - **Method of flux decomposition governed by the eigenvalues Λ^+ and Λ^-**

$$F = P^{-1}(\Lambda^+ + \Lambda^-)PU \tag{18}$$

where $\Lambda^+ = \frac{1}{2}(\Lambda + |\Lambda|)$ and $\Lambda^- = \frac{1}{2}(\Lambda - |\Lambda|)$.

$$\boxed{F_{i-\frac{1}{2},j,k} = \frac{F(U^L_{i-\frac{1}{2},j,k}) + F(U^R_{i-\frac{1}{2},j,k})}{2} + |J|_{i-\frac{1}{2},j,k}\frac{U^L_{i-\frac{1}{2},j,k} - U^R_{i-\frac{1}{2},j,k}}{2}} \tag{19}$$

  - **Jacobien matrix can be evaluated using a formal operators decomposition r_+, r_-, l^+ and l^- (Dutoya approach 1992; extended by Chaouat, 2006)**

$$\boxed{|J|_{i-\frac{1}{2},j,k} = |\lambda^0|I + [\,|\lambda^+| - |\lambda^0|\,]\, r_+ \otimes l^+ + [\,|\lambda^-| - |\lambda^0|\,]\, r_- \otimes l^-} \tag{20}$$

  - **Computation of the Jacobien matrix $J(U)$ using the mathematical property $[a \otimes b]\, U = a\,(b \cdot U)$ where a, b and U are vectors; Vectorized code: 5000 Mflops**

ONERA

NUMERICAL METHOD

- **Numerical scheme in space discretization for solving the convective equations**
  - **Convective flux F at the interface $i-\frac{1}{2},j,k$**

$$F_{i-\frac{1}{2},j,k} = \frac{F(U^L_{i-\frac{1}{2},j,k}) + F(U^R_{i-\frac{1}{2},j,k})}{2} + |J|_{i-\frac{1}{2},j,k}\frac{U^L_{i-\frac{1}{2},j,k} - U^R_{i-\frac{1}{2},j,k}}{2} \quad \textbf{(21)}$$

  - **Computations of $U^{L*}_{i-\frac{1}{2},j,k}$ and $U^C_{i-\frac{1}{2},j,k}$**

$$U^{L*}_{i-\frac{1}{2},j,k} = \frac{-\delta x_{i-1,j,k}U_{i-2,j,k} + (\delta x_{i-2,j,k} + 2\delta x_{i-1,j,k})U_{i-1,j,k}}{\delta x_{i-2,j,k} + \delta x_{i-1,j,k}} \quad \textbf{(22)}$$

$$U^C_{i-\frac{1}{2},j,k} = \frac{\delta x_{i,j,k}U_{i-1,j,k} + \delta x_{i-1,j,k}U_{i,j,k}}{\delta x_{i-1,j,k} + \delta x_{i,j,k}} \quad \textbf{(23)}$$

  - **MUSCL scheme using 5 grid points arround the grid cell i: values U_{i-2}, U_{i-1}, U_i, U_{i+1} et U_{i+2} and requiring the flux limiters Φ**

$$U^L_{i-\frac{1}{2},j,k} = \Phi^L_{i,j,k}U^{L*}_{i-\frac{1}{2},j,k} + (1-\Phi^L_{i,j,k})U^C_{i-\frac{1}{2},j,k} \quad \textbf{(24)}$$

NUMERICAL METHOD

- **Numerical scheme in time discretization for solving the source turbulent equations (Chaouat, 2006)**
  - **Implicitation of source terms that appear in the turbulent equations**

$$\frac{\partial \tau_{ij}}{\partial t} = A[\tau_{ij}] - [Q(\tau_{ij})]\, \tau_{ij} \tag{25}$$

  - **Decomposition of the matrix into a diagonal and a non-diagonal parts**

$$Q = D + R \tag{26}$$

  - **Numerical resolution by the Jacobi method based on iterative algorithm**

$$(\tau_{ij}^{p+1})(I + D[(\tau_{ij}^{p}))]\delta t) = (\tau_{ij}^{n}) + (A[(\tau_{ij}^{p})] - R[(\tau_{ij}^{p})]\,(\tau_{ij}^{p}))\delta t \tag{27}$$

  - **Iterative convergence such as** $(\tau_{ij}^{n+1}) = \lim_{p\to\infty}(\tau_{ij}^{p})$
  - **Condition of positivity for the variables** $\tau_{11}, \tau_{22}, \tau_{33}$

ROTATING CHANNEL FLOWS

- **Field of turbomachinery, compressors and turbines**
- **Navier-Stokes equations in a spanwise rotation frame of reference $\mathbf{\Omega} = (0, 0, \Omega_3)$**

$$\nu \frac{\partial^2 \langle u_1 \rangle}{\partial x_2^2} - \frac{\partial \tau_{12}}{\partial x_2} + \frac{G}{\rho} = 0 \quad (28)$$

$$\frac{1}{\rho} \frac{\partial \langle p \rangle}{\partial x_2} + \frac{\partial \tau_{22}}{\partial x_2} + 2\,\Omega_3\,\langle u_1 \rangle = 0 \quad (29)$$

- **Rupture of the symmetry, apparition of cyclonic and anticyclonic regions**

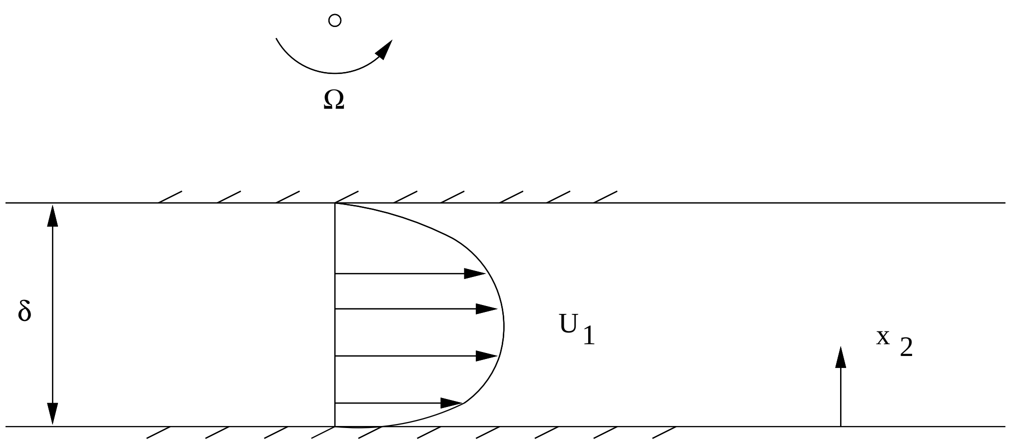

Figure 1: Rotating channel

RSM MODELING FOR ROTATING FLOWS

- **Influence of the Coriolis forces for the τ_{ij} transport equation**

$$\frac{\partial \tau_{ij}}{\partial t} + \langle u_k \rangle \frac{\partial \tau_{ij}}{\partial x_k} = P_{ij} - 2\Omega_p \left(\epsilon_{jpk}\tau_{ki} + \epsilon_{ipk}\tau_{kj} \right) + \Phi_{ij} - \epsilon_{ij} + J_{ij} \qquad \textbf{(30)}$$

- **Turbulent production due to the Coriolis forces** $P^R_{ij} = -2\Omega_p \left(\epsilon_{jpk}\tau_{ki} + \epsilon_{ipk}\tau_{kj} \right)$
- **Mean velocity gradient in the absolute frame of reference, (Speziale et Gatski, 1991)**

$$\frac{D\langle u_k \rangle}{Dx_l} = \frac{\partial \langle u_k \rangle}{\partial x_l} + \epsilon_{kpl}\Omega_p \qquad \textbf{(31)}$$

- **Modeling of the redistribution term, (Chaouat, 2001)** $\Phi^2_{ij} = -c_2 \left(P_{ij} + \frac{1}{2} P^R_{ij} - \frac{2}{3} P\delta_{ij} \right)$
- **Modeling of the implicite rotation effects to the turbulence through the directional structure tensor in the spectral space (Cambon et Jacquin, 1989; Reynolds et Kassinos, 1995; Schiestel, 1997)**
- **Transport equation of the mean vorticity** $\langle \omega_i \rangle = \epsilon_{ijk}\partial \langle u_k \rangle / \partial x_j$

$$\frac{\partial \langle \omega_i \rangle}{\partial t} + \langle u_k \rangle \frac{\partial \langle \omega_i \rangle}{\partial x_k} = \left(\langle \omega_k \rangle + 2\,\Omega_k \right) \frac{\partial \langle u_i \rangle}{\partial x_k} + \nu \frac{\partial^2 \langle \omega_i \rangle}{\partial x_k \partial x_k} - \epsilon_{ipq} \frac{\partial^2 \tau_{qk}}{\partial x_k \partial x_k} \qquad \textbf{(32)}$$

VELOCITY PROFILES

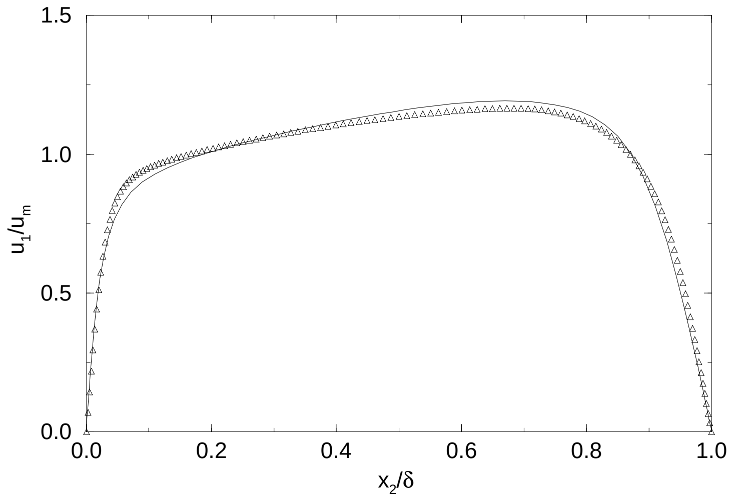

(a)

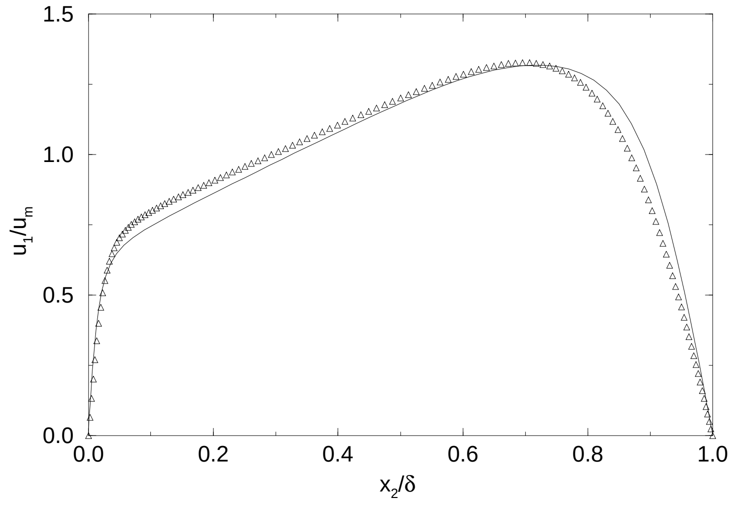

(b)

Figure 2: Mean velocity profile $\langle u_1 \rangle / u_m$ in global coordinate; $\triangle$ DNS; — RSM. anticyclonic wall $x_2/\delta \approx 0$; cyclonic wall $x_2/\delta \approx 1$; (a) R_τ=162, R_O=18; (b) R_τ=162, R_O=6. Symbols: DNS (Lamballais and Lesieur, 1998) ; —–: RSM (Chaouat, 2001); $R_O = 3\, u_m/(\delta\Omega)$.

- **Definition of the Richardson number $R_i = -\Omega_3(S_{12} - \Omega_3)/S_{12}^2$**
- **The mean velocity gradient $\partial \langle u_1 \rangle / \partial x_2 \approx 2\Omega_3$**
- **Absolute vorticity $\langle W_3 \rangle = \langle \omega_3 \rangle + 2\Omega_3 \approx 0$.**

ONERA

TURBULENT STRESS PROFILES

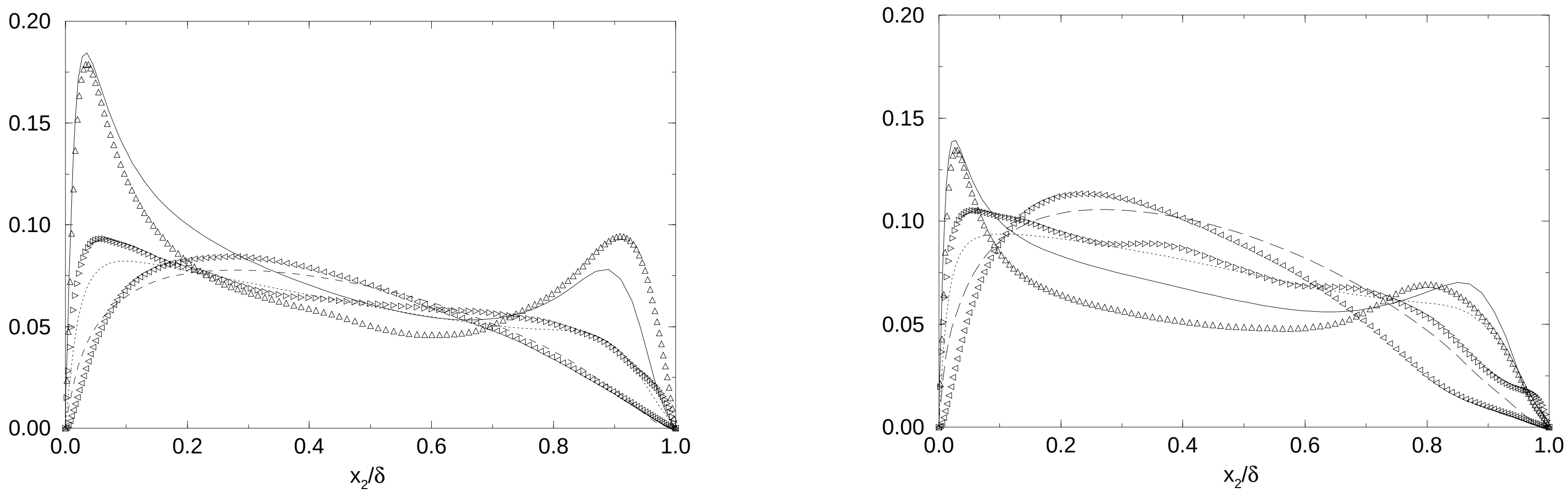

(a) (b)

Figure 3: Turbulent stresses normalized by the bulk velocity in global coordinate. Symbols: DNS; —-: RSM. $\langle u'_1 u'_1 \rangle^{1/2} / u_m$: Δ, —; $\langle u'_2 u'_2 \rangle^{1/2} / u_m$: $\lhd$, - - -; $\langle u'_3 u'_3 \rangle^{1/2} / u_m$: $\rhd$, ...; (a) R_τ=162, R_O=18; (b) R_τ=162, R_O=6.

- **Good agrements with the DNS data (Lamballais and Lesieur, 1998)**
- **Decrease of the turbulent activity in comparison with non-rotating channel flows**
- **New anisotropy distribution in the anticyclonic and cyclonic regions**

SOLUTION TRAJECTORIES

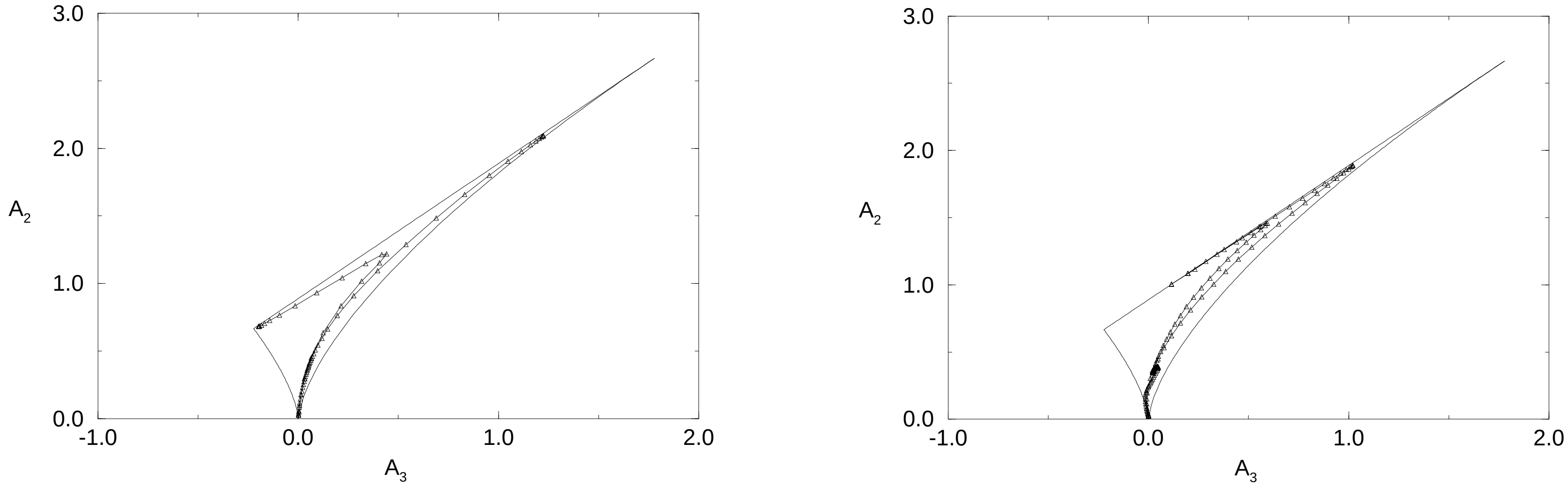

(a) **(b)**

Figure 4: Solution trajectories in fully developed rotating channel flow projected onto the second-invariant/third-invariant plane. (a) DNS; (b) RSM; R_τ=162, R_O=6;

- **The realizalility conditions are satisfied since the curve remains inside the curvilinear triangle**
- **the trajectories are not symmetric when moving from the anticyclonic wall toward the cyclonic wall**

HIGH-LIFT AIRFOIL FLOWS

- Field of aeronautics, design optimization of aircraft wings
- Complex flow physics : strong effects of streamline curvature, adverse presure gradient, transition regime, flow recirculation, attachement and separation of boundary layers
- A-Aérospatiale profile, ONERA data base, LDV (Gleize et al., 1988)

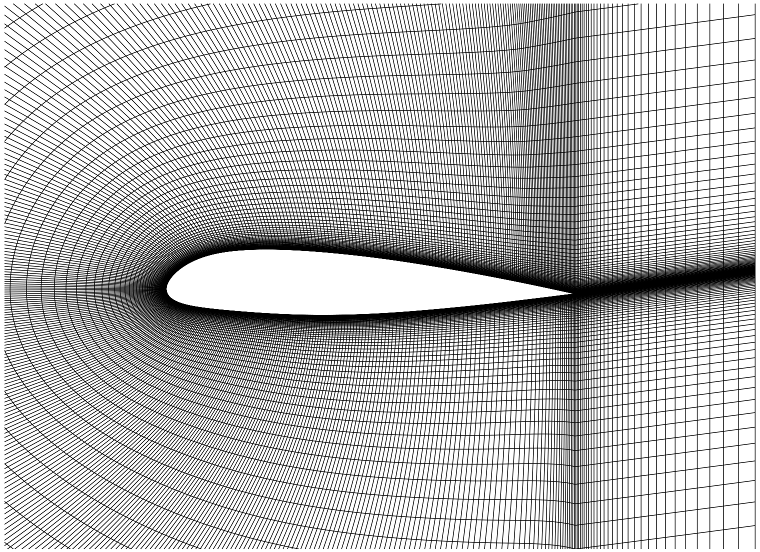

Figure 5: Computational grid 513×97 around the A-airfoil designed by Aéropastiale.

HIGH-LIFT AIRFOIL FLOWS

- **Grid independence solution : 256$\times$ 97; 513$\times$ 97; 1025$\times$ 193 (Chaouat, 2006)**
- **Reynolds $R_c = 2.1\,10^6$; $M_\infty = 0.15$; $u_\infty = 51$ m/s; chord $c = 0.6$ m; $\alpha = 13.3^\circ$**
- **Airfoil flow (numerical properties)**

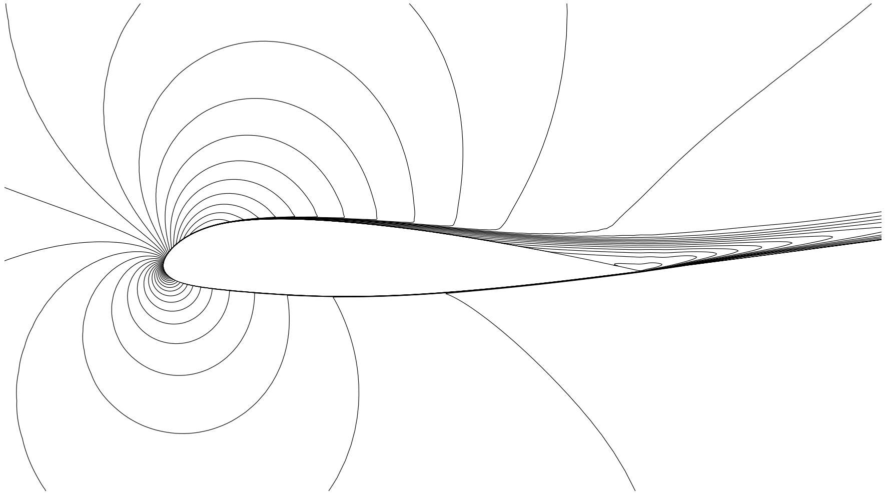

Figure 6: Streamwise velocity contours $\langle u_1 \rangle$ for $\alpha = 13.3^\circ$ incidence angle. RSM computation

PRESSURE CONTOURS

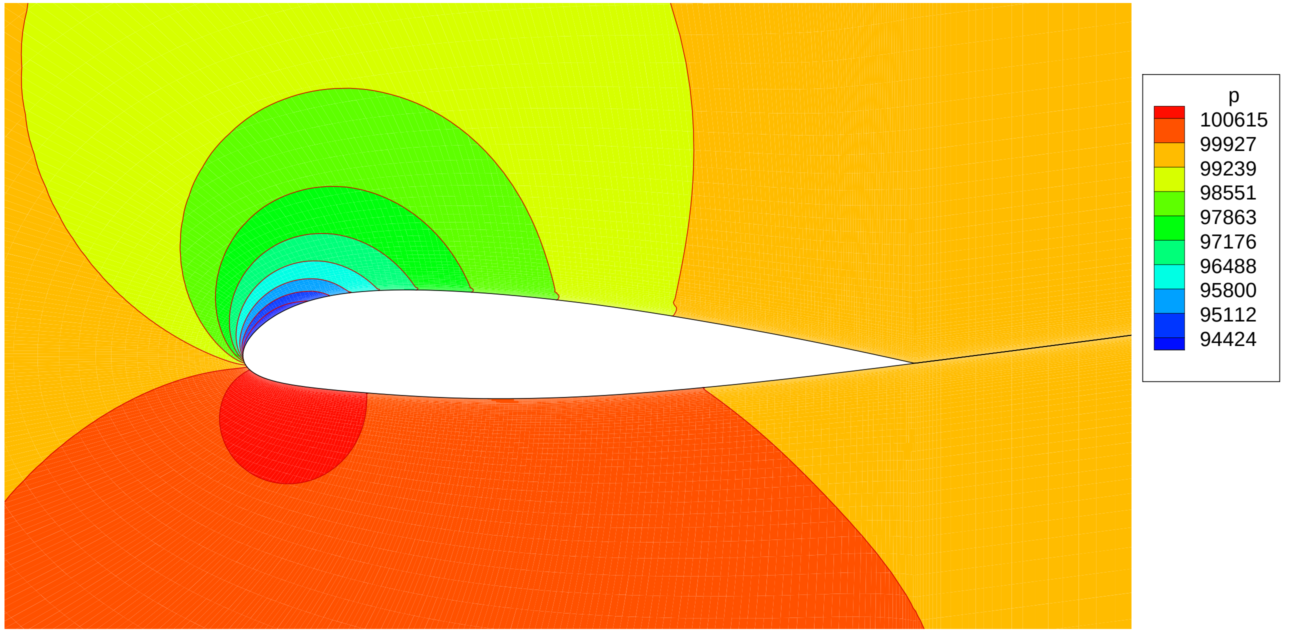

Figure 7: Pressure contours for $\alpha = 13.3^\circ$ incidence angle. Computation RSM.

FRICTION COEFFICIENT $\alpha = 13.3°$.

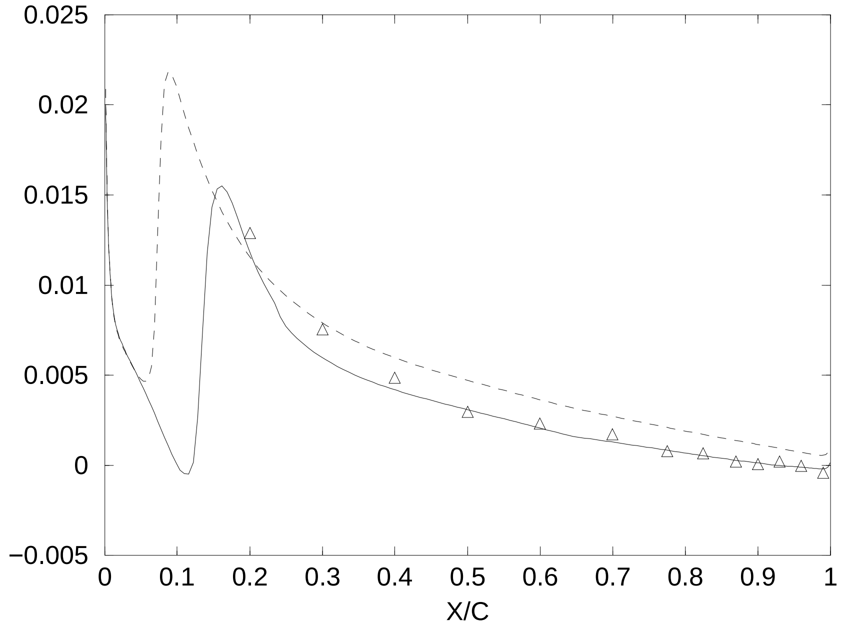

Figure 8: Friction coefficient $C_f = \tau_w/(0.5\rho_\infty u_\infty^2)$ on the suction side. Δ Exp; — RSM; - - $k-\epsilon$. $\alpha = 13.3°$.

- **RSM model is able to predict the laminar separation bubble, turbulent reattachment and turbulent separation near the trailing edge on the suction side (free transition resolution to assess the performances of the turbulence models)**

PRESSURE COEFFICIENT $\alpha = 13.3°$.

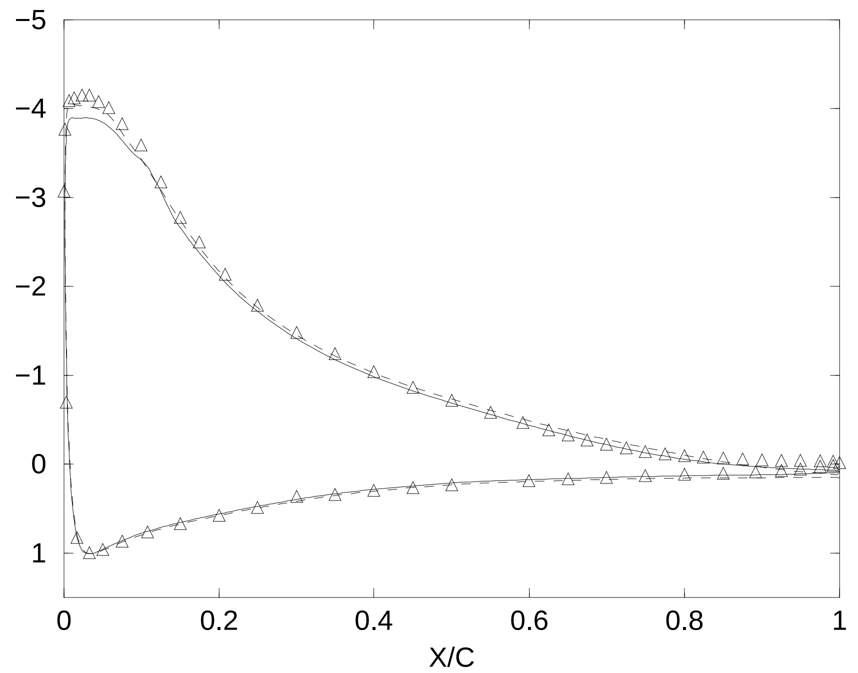

Figure 9: Pressure coefficient $C_p = (p - p_\infty)/(0.5\rho_\infty u_\infty^2)$ around the airfoil. Δ Exp; — RSM ; - - $k - \epsilon$. $\alpha = 13.3°$.

- **The leading edge pressure peak on the suction side where the flow is laminar appears too low for the RSM computation. The $k - \epsilon$ computation overpredicts the measurements in the region that extends from the transition location to the trailing edge**

VELOCITY PROFILES $\alpha = 13.3°$.

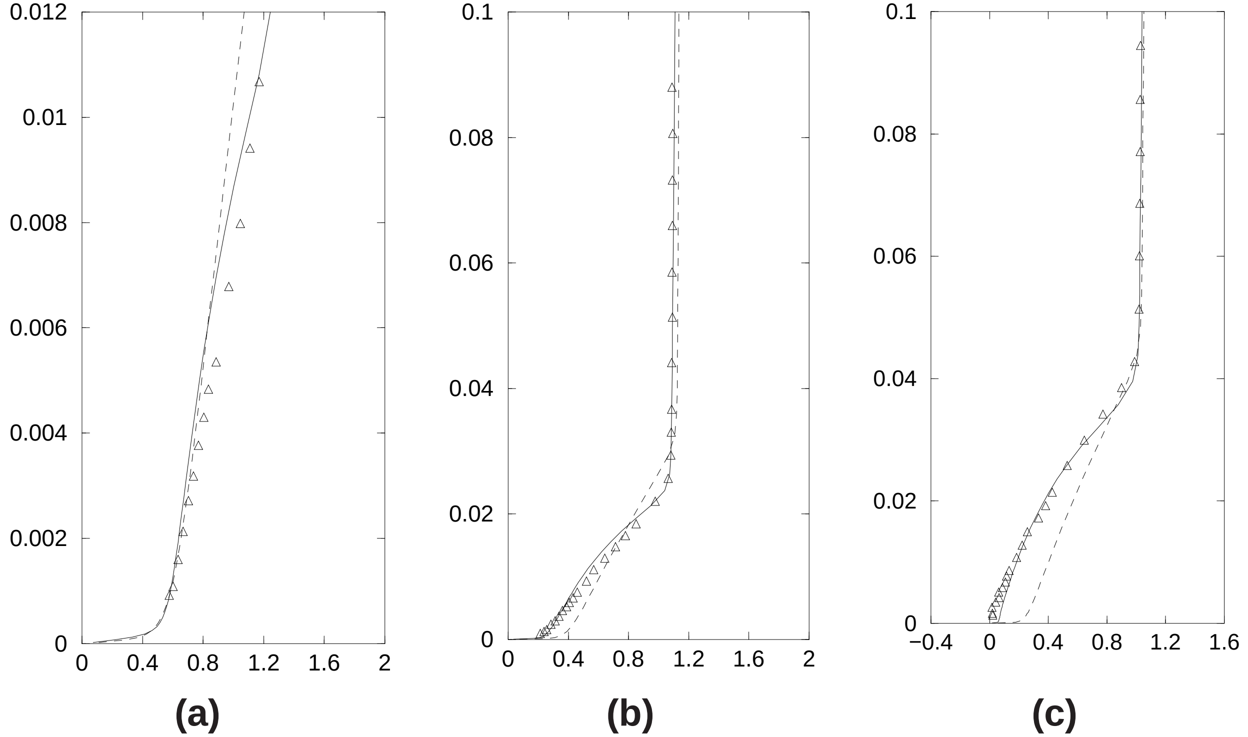

Figure 10: Mean velocity profiles $\langle u_1 \rangle / u_\infty$. (a) x/c=0.5 ; (b) x/c=0.7 ; (c) x/c=0.825. Δ Exp; — RSM; - - $k - \epsilon$. $\alpha = 13.3°$.

- **RSM model yields a good estimate of the boundary layer thickness contrary to $k - \epsilon$ model that underpredicts the measurements and provides too high velocities.**

TURBULENT STRESS PROFILES $\alpha = 13.3°$.

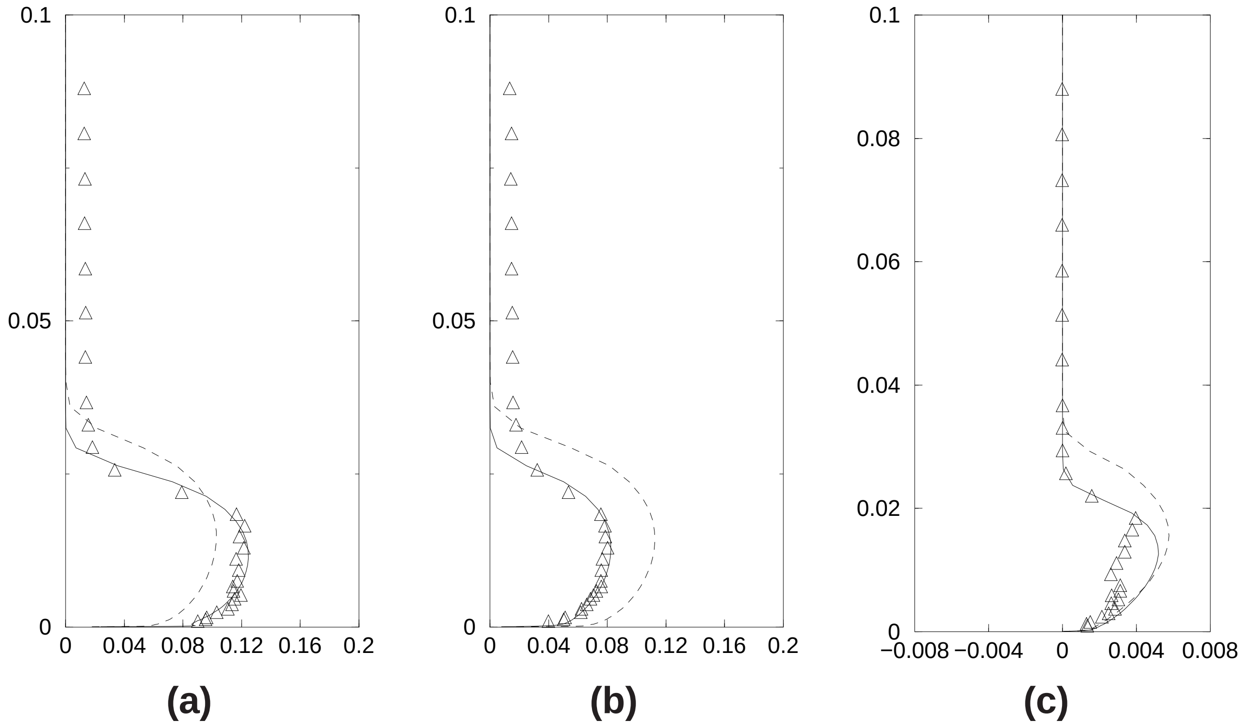

Figure 11: Turbulent stress profiles at x/c=0.7. Δ Exp; — RSM; - - $k - \epsilon$; (a) $\sqrt{\tau_{11}}/u_\infty$; (b) $\sqrt{\tau_{22}}/u_\infty$; (c) τ_{12}/u_∞^2. $\alpha = 13.3°$.

- **Good RSM agreement with the experiment in the attached boundary layer**

ONERA

TURBULENT STRESS PROFILES $\alpha = 13.3°$.

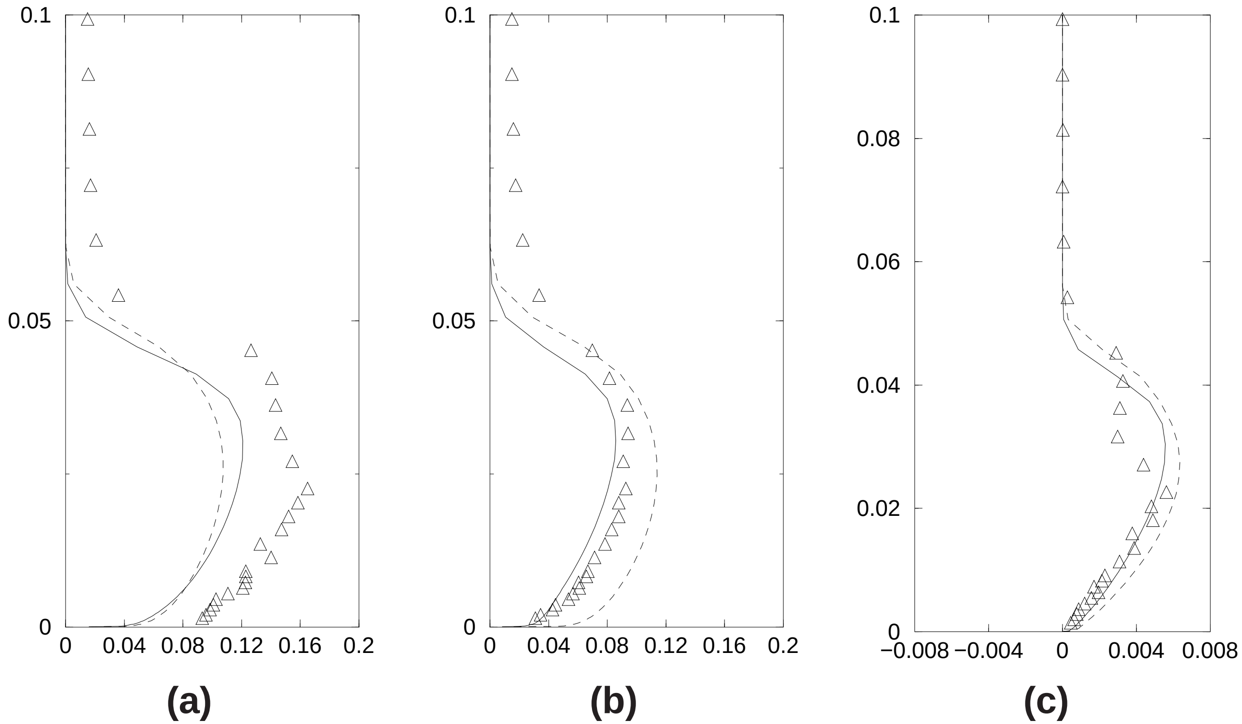

Figure 12: Turbulent stress profiles at à x/c=0.87. Δ Exp; — RSM; - - $k - \epsilon$; (a) $\sqrt{\tau_{11}}/u_\infty$; (b) $\sqrt{\tau_{22}}/u_\infty$; (c) τ_{12}/u_∞^2. $\alpha = 13.3°$.

- **Good RSM agreement with the experiment in the detached boundary layer**

ONERA

STREAMLINE CONTOURS $\alpha = 13.3^\circ$.

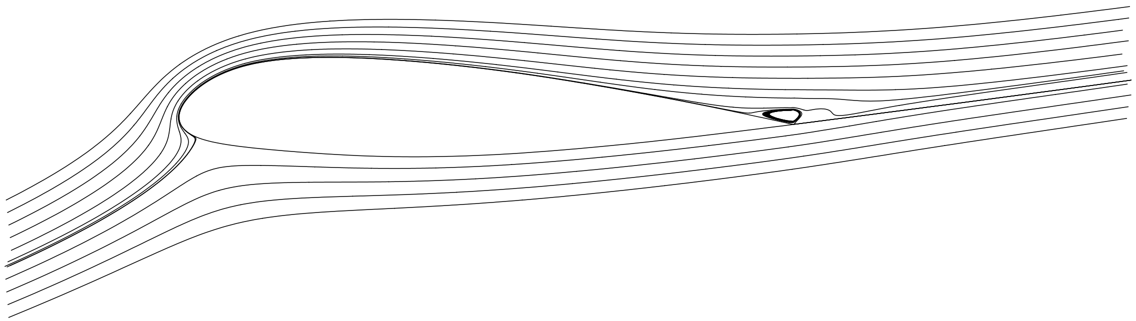

Figure 13: Streamline contours for $\alpha = 13.3^\circ$ incidence angle. RSM computation.

- Detachment of the boundary layer on the suction side
  - Redistribution term Φ_{ij} that reproduces the anisotropy
  - Use of the function $\psi = A(P/\epsilon - 1)$ in the dissipation-rate equation that takes into account non-equilibrium turbulence

TRANSPOSITION OF RSM MODELS TO HYBRID/LES MODELS

- **Cooperation between ONERA and IRPHE (Roland Schiestel)**
  - **Spectral partitioning (m = number of zones), definition of filtered and averaged quantities**

$$u_i = \langle u_i \rangle + \sum_{m=1}^{N} u_i^{\prime(m)} \; ; \; u_i^{\prime(m)}(\boldsymbol{\xi}) = \int_{\kappa_{m-1}<|\kappa|<\kappa_m} \widehat{u'}_i(\boldsymbol{\kappa}) \exp\left(j\boldsymbol{\kappa}\boldsymbol{\xi}\right) d\boldsymbol{\kappa} \qquad \textbf{(33)}$$

  - **Simulation LES (m=2) : filtered velocity:** $\bar{u}_i = \langle u_i \rangle + u_i^{\prime(1)}$
    - **Large-scale fluctuating velocity:** $u_i^{<} = u_i^{\prime(1)}$
    - **subgrid-scale fluctuating velocity:** $u_i^{>} = u_i^{\prime(2)}$

MATHEMATICAL PHYSICS FORMALISM IN THE SPECTRAL SPACE

- Two-point velocity fluctuating correlation for non-homogeneous turbulence
  $\tau_{ij} = \left\langle u'_{iA} u'_{jB} \right\rangle (\boldsymbol{X}, \boldsymbol{\xi})$
- Taylor series development for the mean velocity (framework of tangent homogeneous spectral space)
- Fourier transform of the transport equation for the tensor $\tau_{ij} = \left\langle u'_{iA} u'_{jB} \right\rangle$
- Integration on a spherical shell in the wave numbers (Cambon, 1992)

$$\varphi_{ij}(\kappa, \boldsymbol{X}) = \left(\tau_{ij}(\boldsymbol{X}, \boldsymbol{\xi})\right)^{\Delta} = \frac{1}{A(\kappa)} \iint_{\partial A} \widehat{\tau_{ij}}(\boldsymbol{\kappa}, \boldsymbol{X}) dA(\boldsymbol{\kappa}) \qquad (34)$$

- Resulting equation in the spectral space, (Chaouat and Schiestel, 2007)

$$\frac{D\varphi_{ij}(\boldsymbol{X}, \kappa)}{Dt} = \mathcal{P}_{ij}(\boldsymbol{X}, \kappa) + \mathcal{T}_{ij}(\boldsymbol{X}, \kappa) + \Pi_{ij}(\boldsymbol{X}, \kappa) + \mathcal{J}_{ij}(\boldsymbol{X}, \kappa) - \mathcal{E}_{ij}(\boldsymbol{X}, \kappa) \qquad (35)$$

MATHEMATICAL PHYSICS FORMALISM IN THE SPECTRAL SPACE

- **Resulting equation in the spectral space, (Chaouat and Schiestel, 2007)**

$$\frac{D\varphi_{ij}(\boldsymbol{X},\kappa)}{Dt} = \mathcal{P}_{ij}(\boldsymbol{X},\kappa) + \mathcal{T}_{ij}(\boldsymbol{X},\kappa) + \Pi_{ij}(\boldsymbol{X},\kappa) + \mathcal{J}_{ij}(\boldsymbol{X},\kappa) - \mathcal{E}_{ij}(\boldsymbol{X},\kappa) \tag{36}$$

- **Physical meaning : production, transfer, redistribution, diffusion and dissipation-rate**
- **Expressions of these terms can be obtained exactly. For instance, the transfer term takes the following form:**

$$\mathcal{T}_{ij}(\boldsymbol{X},\kappa) = -\left[\left(\frac{\partial}{\partial \xi_k}\left[\langle u'_{i_A} u'_{k_B} u'_{j_B}\rangle - \langle u'_{i_A} u'_{k_A} u'_{j_B}\rangle\right]\right)^{\Delta} + \left(\xi_m \frac{\partial \tau_{ij}}{\partial \xi_k}\right)^{\Delta} \frac{\partial \langle u_k \rangle}{\partial X_m}\right] \tag{37}$$

MATHEMATICAL PHYSICS FORMALISM IN THE SPECTRAL SPACE

- **Integration in the spectral space for recovering physical space quantities**
  - **Statistical one-scale models in the physical space**

$$\tau_{ij} = \int_0^\infty \varphi_{ij}(\boldsymbol{X},\kappa)d\kappa \quad => \quad \frac{D\tau_{ij}}{Dt} = P_{ij} + \Phi_{ij} + J_{ij} - \epsilon_{ij} \tag{38}$$

  - **Statistical multiple-scale models in the physical space, (Schiestel, 1987)**

$$\tau_{ij}^{(m)} = \int_{\kappa_{m-1}}^{\kappa_m} \varphi_{ij}(\boldsymbol{X},\kappa)d\kappa \quad => \quad \frac{D\tau_{ij}^{(m)}}{Dt} = P_{ij}^{(m)} + F_{ij}^{(m-1)} - F_{ij}^{(m)} + \Phi_{ij}^{(m)} + J_{ij}^{(m)} - \epsilon_{ij}^{(m)} \tag{39}$$

  - **Subgrid-scale models in the physical space, (Chaouat and Schiestel, 2005)**

$$\langle(\tau_{ij})_{sgs}\rangle = \langle u_i^> u_j^> \rangle = \tau_{ij}^{(2)} \quad => \quad \frac{D\langle(\tau_{ij})_{sgs}\rangle}{Dt} = P_{ij}^{(2)} + F_{ij}^{(1)} - F_{ij}^{(2)} + \Phi_{ij}^{(2)} + J_{ij}^{(2)} \tag{40}$$

by analogy :

$$\frac{D(\tau_{ij})_{sgs}}{Dt} = ... \tag{41}$$

CONTINUOUS HYBRID RANS/LES MODEL (PITM)

- **Modeled transport equation for the subgrid-scale stress tensor**

$$\boxed{\frac{D(\tau_{ij})_{sgs}}{Dt} = (P_{ij})_{sgs} - (\epsilon_{ij})_{sgs} + (\Phi_{ij})_{sgs} + (J_{ij})_{sgs}} \quad \textbf{(42)}$$

$$(P_{ij})_{sgs} = -(\tau_{ik})_{sgs}\frac{\partial \bar{u}_j}{\partial x_k} - (\tau_{jk})_{sgs}\frac{\partial \bar{u}_i}{\partial x_k} \quad \textbf{(43)}$$

$$(\epsilon_{ij})_{sgs} = \frac{2}{3}\epsilon_{sgs}\delta_{ij} \quad \textbf{(44)}$$

  – **Modeling for the terms $(\Phi_{ij})_{sgs}$ and ϵ_{sgs}**

  – **Universal functions dependent on the dimensionless parameter $\eta_c = \kappa_c L_e$ involving the turbulent length scale**

$$\boxed{L_e = \frac{k^{3/2}}{(\epsilon_{sgs} + \epsilon^{<})}} \quad \textbf{(45)}$$

  * $u_i = \bar{u}_i + u_i^{>} = (\langle u_i \rangle + u_i^{<}) + u_i^{>}$
  * $k = k_{sgs} + k_{les}$
  * $\kappa_c = \pi/\Delta = \pi/(\Delta_1\Delta_2\Delta_3)^{1/3}$
  * $\epsilon^{<} = \nu(\partial u_i^{<} \partial u_i^{<} / \partial x_j \partial x_j)$

ONERA

CONTINUOUS HYBRID RANS/LES MODEL (PITM)

- **Modeling of the redistribution term**
  - **Slow term of return to isotropy function of the splitting cutoff**

$$(\Phi^2_{ij})_{sgs}(\eta_c) = -c_{sgs_1}(\eta_c)\frac{\epsilon_{sgs}}{k_{sgs}}\left((\tau_{ij})_{sgs} - \frac{1}{3}(\tau_{mm})_{sgs}\delta_{ij}\right) \quad \textbf{(46)}$$

$$c_{sgs_1}(\eta_c) = \frac{1+\alpha_\eta\,\eta_c^2}{1+\eta_c^2}c_1 \qquad (\textbf{empirical constant } \alpha_\eta = 1.5) \quad \textbf{(47)}$$

  - **Rapid term of return to isotropy function of the filtered velocity gradient**

$$(\Phi^1_{ij})_{sgs} = -c_2\left((P_{ij})_{sgs} - \frac{1}{3}(P_{mm})_{sgs}\delta_{ij}\right) \quad \textbf{(48)}$$

- **Analogy with the the multiple-scale models (Schiestel, 1987)**

CONTINUOUS HYBRID RANS/LES MODEL (PITM)

- **Modeling of the dissipation-rate equation by a mathematical physics formalism in the spectral space**
  - **Resulting equation in the physical space, (Chaouat and Schiestel, 2007)**

$$\frac{D\tau_{ij}^{(m)}}{Dt} = P_{ij}^{(m)} + F_{ij}^{(m-1)} - F_{ij}^{(m)} + \Phi_{ij}^{(m)} + J_{ij}^{(m)} - \epsilon_{ij}^{(m)} \quad \textbf{(49)}$$

where

$$F_{ij}^{(m)} = \mathcal{F}_{ij}^{(m)} - \varphi_{ij}(\boldsymbol{X},\kappa)\frac{\partial \kappa_m}{\partial t} \quad \textbf{and} \quad \mathcal{F}_{ij}^{(m)} = -\int_0^{\kappa_m} \mathcal{T}_{ij}(\boldsymbol{X},\kappa)d\kappa, \quad \textbf{(50)}$$

  - **Dimensionless relation between the splitting wavenumber $\kappa_2 = \kappa_d$ located after the inertial range and the cutoff wavenumber $\kappa_1 = \kappa_c$**

$$\kappa_d - \kappa_c = \zeta_{sgs}\frac{\epsilon_{sgs}}{{k_{sgs}}^{3/2}} \quad \textbf{(51)}$$

  - **Derivative of equation (51) using equation (49) in its contracted form then yields**

$$\frac{D\epsilon_{sgs}}{Dt} = c_{\epsilon_1}\frac{\epsilon_{sgs}}{k_{sgs}}\frac{(P_{mm})_{sgs}}{2} - c_{sgs\epsilon_2}(\eta_c)\frac{\epsilon_{sgs}^2}{k_{sgs}} + (J_\epsilon)_{sgs} \quad \textbf{(52)}$$

CONTINUOUS HYBRID RANS/LES MODEL (PITM)

- **Coefficient $c_{sgs\epsilon_2}$ is function of the cutoff wave-number as a result of the analytical theory (Chaouat and Schiestel, 2005)**

$$c_{sgs\epsilon_2}(\eta_c) = c_{\epsilon_1} + \frac{k_{sgs}}{k}(c_{\epsilon_2} - c_{\epsilon_1}) \tag{53}$$

  - **Computation of the subgrid-scale energy in the inertial range $[\kappa_c, +\infty[$, $k_{sgs} = \int_{\kappa_c}^{\infty} E(\kappa) d\kappa$**
  - **New accurate energy spectrum inspired by Von Karman type spectra valid on the entire range of wavenumbers**

$$\boxed{E(\kappa) = \frac{\frac{2}{3}\beta_\eta L_e^3\, k\, \kappa^2}{\left[1 + \beta_\eta(\kappa\, L_e)^3)\right]^{11/9}}} \tag{54}$$

where β_η is a constant coefficient, instead of simply referring to the Kolmogorov law valid in the inertial range $E(\kappa) = C_K \epsilon^{2/3} \kappa^{-5/3}$ as made previously

CONTINUOUS HYBRID RANS/LES MODEL (PITM)

- **Analytical computation of the subgrid-scale energy**

$$k_{sgs} = \int_{\kappa_c}^{\infty} E(\kappa) d\kappa = \frac{k}{\left[1+\beta_\eta (\kappa_c L_e)^3)\right]^{2/9}} \quad \textbf{(55)}$$

- **Exact expression of the coefficient c_{ϵ_2}**

$$\boxed{c_{sgs\epsilon_2}(\eta_c) = c_{\epsilon_1} + \frac{c_{\epsilon_2} - c_{\epsilon_1}}{\left[1+\beta_\eta \, \eta_c^3\right]^{2/9}}} \quad \textbf{(56)}$$

where $c_{\epsilon_1} = 1.4$ **and** $c_{\epsilon_2} = 1.9$**.**

- **Limiting behavior**

$\lim_{\eta_c \to 0} c_{sgs\epsilon_2}(\eta_c) = c_{\epsilon_2}$ **(RSM),** $\lim_{\eta_c \to \infty} c_{sgs\epsilon_2}(\eta_c) = c_{\epsilon_1}$ **(DNS)**

CONTINUOUS HYBRID RANS/LES MODELS (PITM)

- **Summary of the PITM models with their practical formulations**
  - **Turbulent stress subfilter model based on the transport equations for $(\tau_{ij})_{sgs}$ and ϵ_{sgs}**

$$\frac{D(\tau_{ij})_{sgs}}{Dt} = (P_{ij})_{sgs} - (\epsilon_{ij})_{sgs} + (\Phi_{ij})_{sgs} + (J_{ij})_{sgs} \quad \textbf{(57)}$$

$$\frac{D\epsilon_{sgs}}{Dt} = c_{\epsilon_1} \frac{\epsilon_{sgs}}{k_{sgs}} \frac{(P_{mm})_{sgs}}{2} - c_{sgs\epsilon_2}(\eta_c) \frac{\epsilon^2_{sgs}}{k_{sgs}} + (J_\epsilon)_{sgs} \quad \textbf{(58)}$$

  - **Turbulent energy subfilter model based on the transport equations for k_{sgs} and ϵ_{sgs}**

$$\frac{Dk_{sgs}}{Dt} = P_{sgs} + J_{sgs} - \epsilon_{sgs} \quad \textbf{(59)}$$

  - **"Exact " coefficient c_{ϵ_2}**

$$c_{sgs\epsilon_2}(\eta_c) = c_{\epsilon_1} + \frac{c_{\epsilon_2} - c_{\epsilon_1}}{[1 + \beta_\eta \, \eta_c^3]^{2/9}} \quad \textbf{(60)}$$

  - **Dimensionless parameter** $\eta_c = (k^{3/2}\kappa_c)/(\epsilon_{sgs} + \epsilon^<)$

CONTINUOUS HYBRID RANS/LES MODELS (PITM)

- **Limiting behavior for the subgrid-scale viscosity model**

$$\frac{k_{sgs}^{3/2}}{\epsilon_{sgs}} = \frac{k^{3/2}}{\epsilon_{sgs}} \left(\frac{k_{sgs}}{k}\right)^{3/2} \quad \textbf{(61)}$$

- **Limiting value** $k_{sgs}/k \approx 3/2C_k\eta_c^{-2/3}$ **when** $k_{sgs} \ll k$

$$k_{sgs}^{3/2}/\epsilon_{sgs} = (3C_K/2)^{3/2}\,\Delta/\pi \quad \textbf{(62)}$$

- **Hypothesis of equilibrium** $\epsilon_{sgs} = 2\nu_{sgs}\left\langle \bar{S}_{i,j}\bar{S}_{i,j}\right\rangle$ **where** $\bar{S}_{ij} = (\partial\bar{u}_i/\partial x_j + \partial\bar{u}_j/\partial x_i)/2$

$$\boxed{\nu_{sgs} = \frac{1}{\pi^2}\left(\frac{3C_K}{2}\right)^3 c_\nu^{3/2}\Delta^2\left[2\left\langle \bar{S}_{ij}\bar{S}_{ij}\right\rangle\right]^{1/2}} \quad \textbf{(63)}$$

- **Limiting behavior for the subgrid viscosity** ν_{sgs} **is simply the Smagorinsky model**

PARTIALLY INTEGRATED TURBULENCE MODEL (PITM)

- Transport equations for k_{sgs} and ϵ_{sgs} (Dejoan and Schiestel, 2002)
- Transport equations for $(\tau_{ij})_{sgs}$ and ϵ_{sgs} (Chaouat and Schiestel, 2005)
- LES simulation for coarse grids
- Non-equilibrium turbulence spectra : unsteady flows or mixing turbulent fields
- Advantages of RSM models are worth to be transposed to subgrid-scale modeling
- Self consistency of the model obtained when the cutoff location is continuous varied
- The model guaranties compatibility with the two extreme limits that are the full statistical Reynolds stress transport model and DNS
- Bridge between URANS and LES method with seamless coupling
- Consistency

$$\lim_{\kappa_c \to 0} [(\tau_{ij})_{sgs}] = (\tau_{ij})_{RANS} \tag{64}$$

SIMULATION OF HOMOGENEOUS TURBULENCE

- **Decay of isotropic non-perturbed spectrum using the two-equation subfilter model**
  - Comte-Bellot and Corrsin experiment at low Reynolds number
  - PITM simulation performed on a medium grid $N = 80^3$ for a box-size $L = 1.256$ m
  - Wave-numbers defined by $\kappa = 2\pi/n$ where n varies from $-N/2+1$ to $N/2$ leading to $\kappa_{min} = 2\pi/(N\Delta) = 0.05$ cm^{-1} and $\kappa_{max} = \pi/\Delta = 2$ cm^{-1}
  - Ratio of the subgrid energy to the total energy $k_{sgs}/k \approx 1/3$
  - Initial velocity field produced from a random generator (Roy, 1980) enforcing the given energy spectrum
  - Experiment available for the initial time ($tU_0/M =$42) and for the two time advancements ($tU_0/M =$98, 171)

SIMULATION OF DECAY OF HOMOGENEOUS TURBULENCE

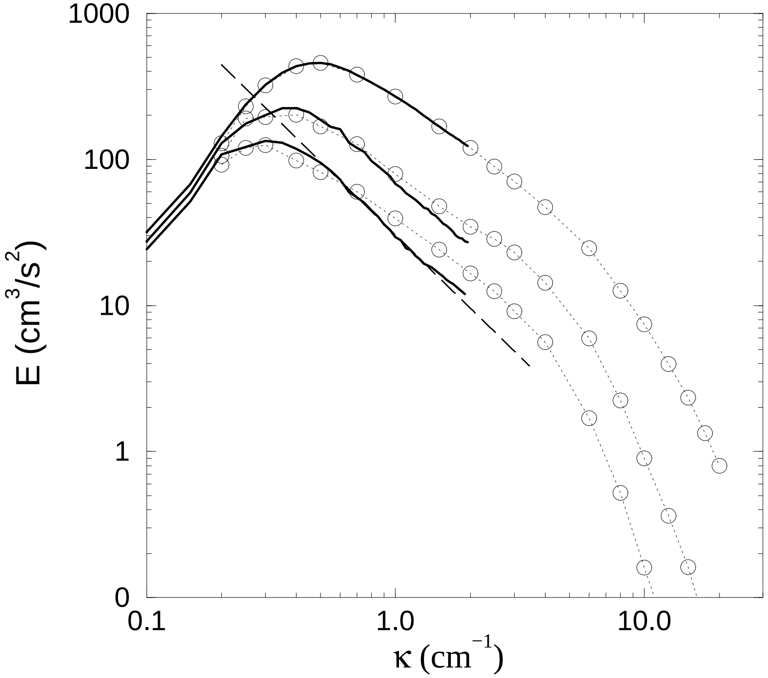

Figure 14: Homogeneous decay of the energy spectra ($\kappa_c = 2$ cm^{-1}). $\cdots$ ○ $\cdots$: Comte-Bellot experiment ($t\,U0/M$ =42, 98 and 171); - - : Kolmogorov spectrum with $-5/3$ slope; —: PITM simulation.

- **Good agreement with experimental data for tU_0/M =98 but slightly deviation for tU_0/M =171; Agreement with the $\kappa^{-5/3}$ Kolmogorov slope**

ONERA

DECAY WITH A PERTURBED INITIAL SPECTRUM

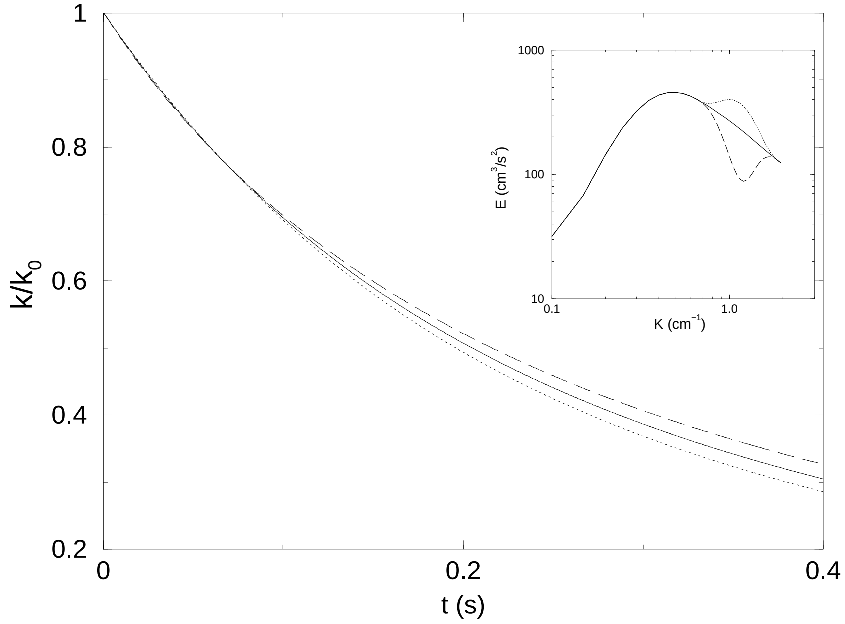

Figure 15: Homogeneous decay of the turbulent energy $k/k_0 = (k_{sgs} + k_{les})/k_0$; $\kappa_c = 2$ cm^{-1}; (α) : —; (β) ...; (γ) - - -.

- **A peak in large scale energy (resp. a defect in large scale energy) implies a decrease (resp. an increase) of the decay rate of turbulence in agreement with EDQNM spectral model prediction (Cambon et al., 1981)**
- **The small-scale energy decreases more rapidly than the large-scale energy by viscous dissipation**

SIMULATION OF FULLY-TURBULENT CHANNEL FLOWS

- **Periodicity conditions in the streamwise and spanwise directions**
- **No slip condition in the normal direction to the wall**
- **Implementation of a pressure gradient term to balance the viscosity forces**
  - $16 \times 32 \times 64 = 32\,768$ **grid points**
  - $32 \times 64 \times 84 = 172\,032$ **grid points**
  - **Spacings Δ_i in the streamwise and spanwise directions:** $\Delta_1^+ = 50.9$**,** $\Delta_2^+ = 25.1$
  - **Spacing refinement near the walls : dimensionless distance** $\Delta_3^+ = 0.5$
- **Comparison with DNS (Moser et al., 1999) at** $R_\tau = 395$
  - **statistic for the resolved scales :** $\langle(\tau_{ij})_{les}\rangle = \langle\bar{u}_i\bar{u}_j\rangle - \langle\bar{u}_i\rangle\langle\bar{u}_j\rangle$
  - **total stress :** $\tau_{ij} = \langle(\tau_{ij})_{sgs}\rangle + \langle(\tau_{ij})_{les}\rangle$

SUBGRID-SCALE STRESSES

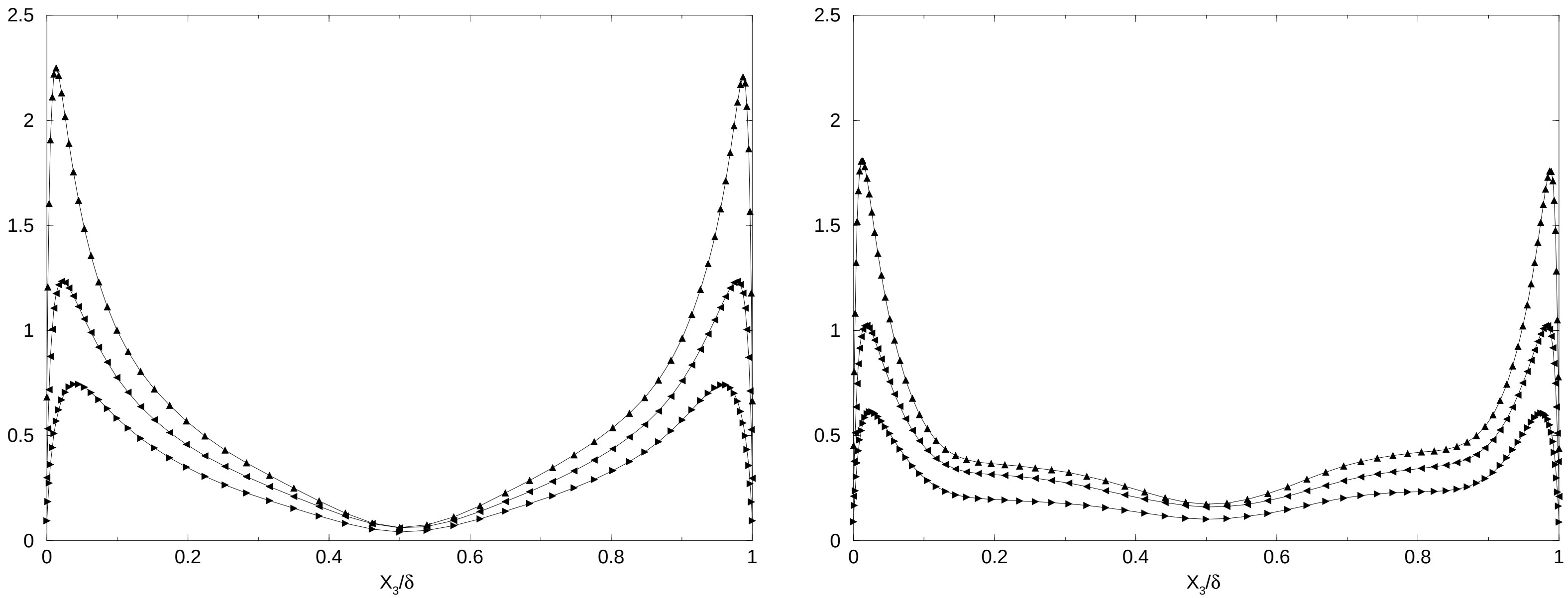

(a) **(b)**

Figure 16: Turbulent subgrid-scale stresses $< (\tau_{ii})^{1/2}_{sgs} > /u_\tau$**. (a) LES 1; (b) LES 2;** $\blacktriangle : i = 1$**,** $\blacktriangleleft : i = 2$**,** $\blacktriangleright : i = 3$**.** $R_\tau = 395$**.**

LARGE-SCALE STRESSES

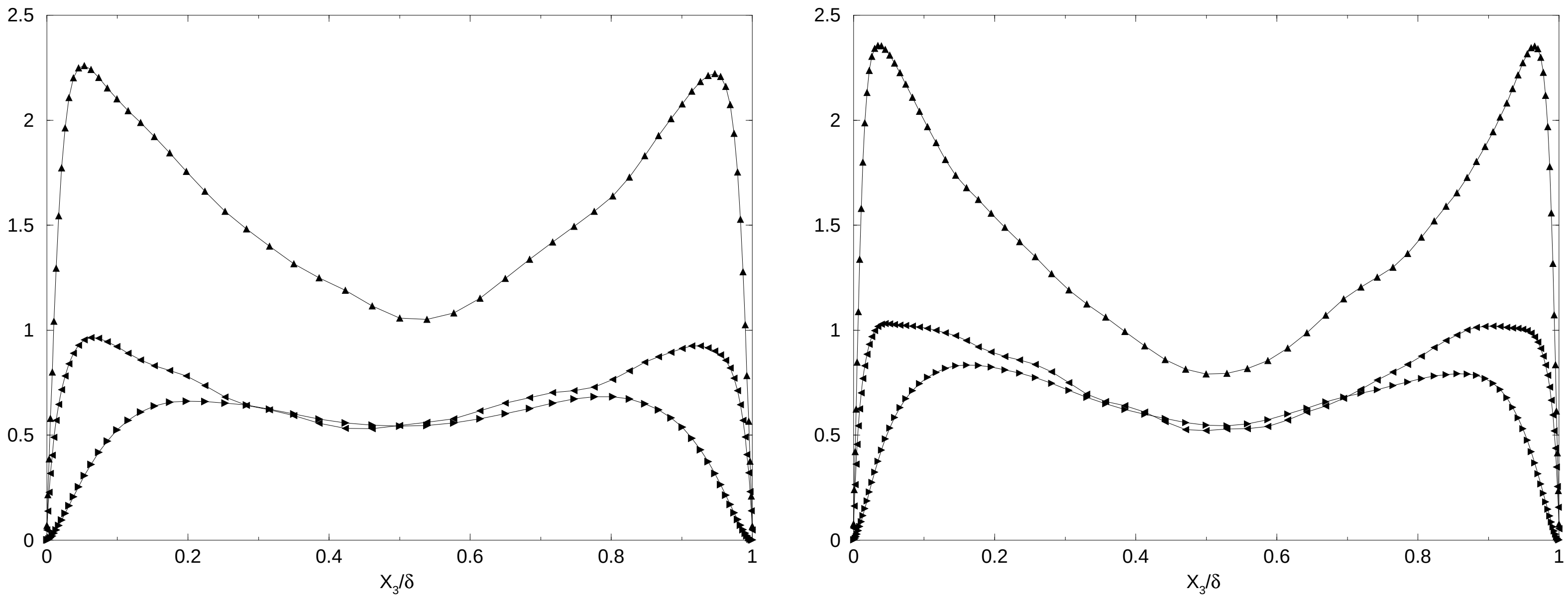

(a) **(b)**

Figure 17: Turbulent large scale stresses $< (\tau_{ii})_{les}^{1/2} > /u_\tau$**. (a) LES 1; (b) LES 2;** $\blacktriangle : i = 1$**,** $\blacktriangleleft$: $i = 2$, $\blacktriangleright$: $i = 3$. $R_\tau = 395$.

REYNOLDS STRESSES

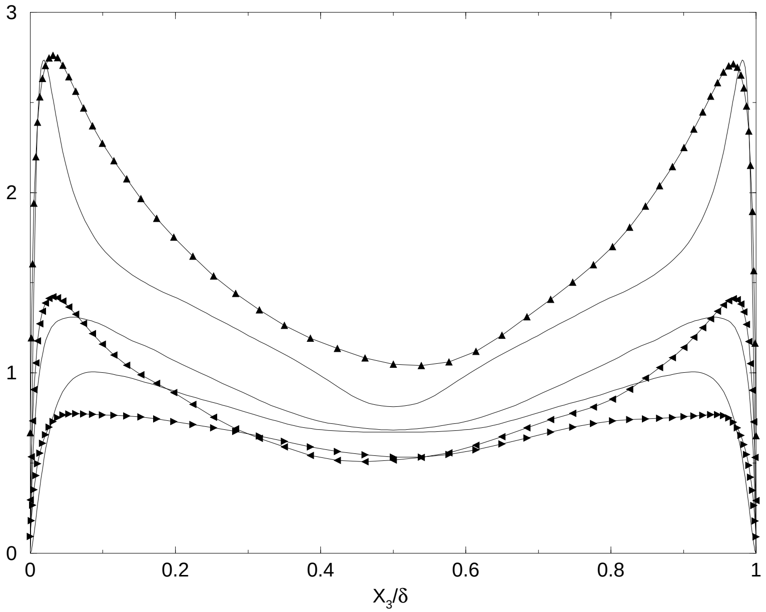

(a)

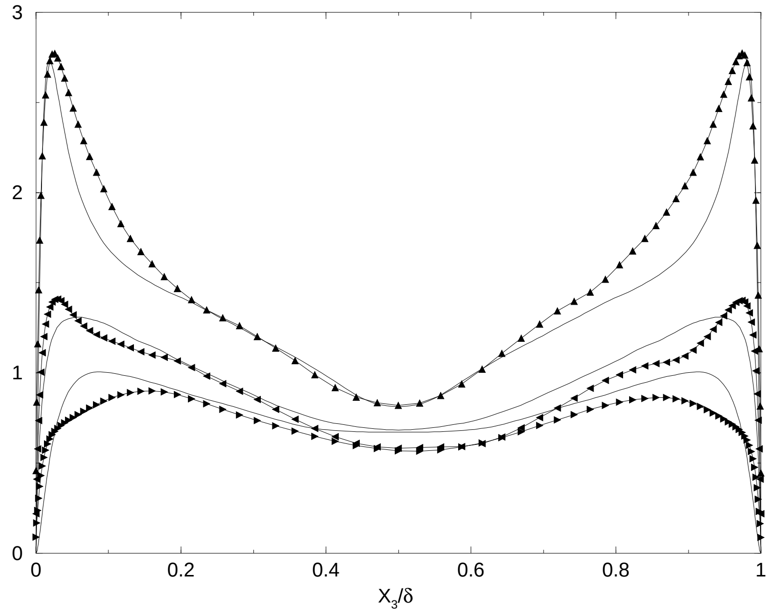

(b)

Figure 18: Turbulent Reynolds stresses $(< (\tau_{ii})_{sgs} > + < (\tau_{ii})_{les} >)^{\frac{1}{2}} / u_\tau$**. (a) LES 1; (b) LES 2; ▲ :** $i = 1$**, ◀:** $i = 2$**, ▶:** $i = 3$**; —: DNS.** $R_\tau = 395$**.**

SUBGRID AND RESOLVED SHEAR STRESSES

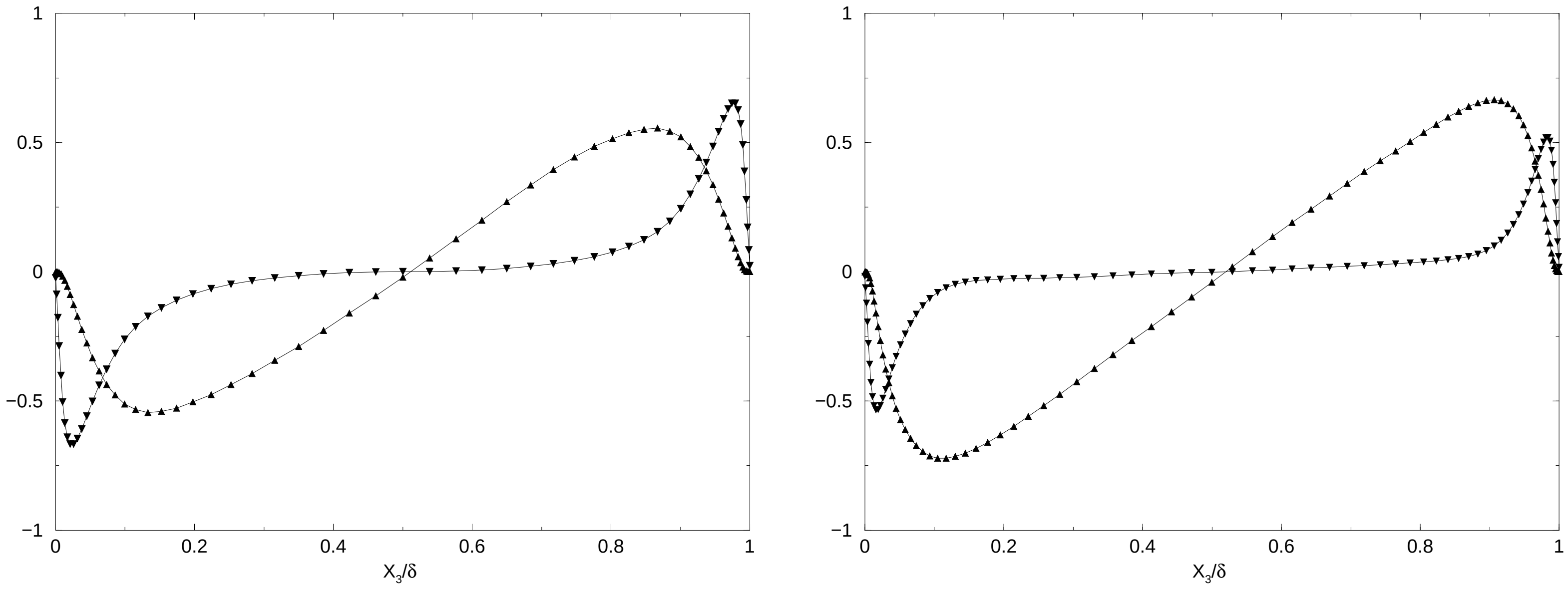

(a) coarse mesh **(b) medium mesh**

Figure 19: Turbulent subgrid-scale stress $<(\tau_{13})_{sgs}>/u_\tau$ **and resolved scale stress** $<(\tau_{13})_{les}>/u_\tau$**. (a) LES 1; (b) LES 2; ▼:SGS; ▲: LES;** $R_\tau = 395$**.**

- **Sharing out of turbulence energy among the subgrid and resoved turbulence scales for different meshes**

ONERA – 8/2014

TOTAL SHEAR STRESSES

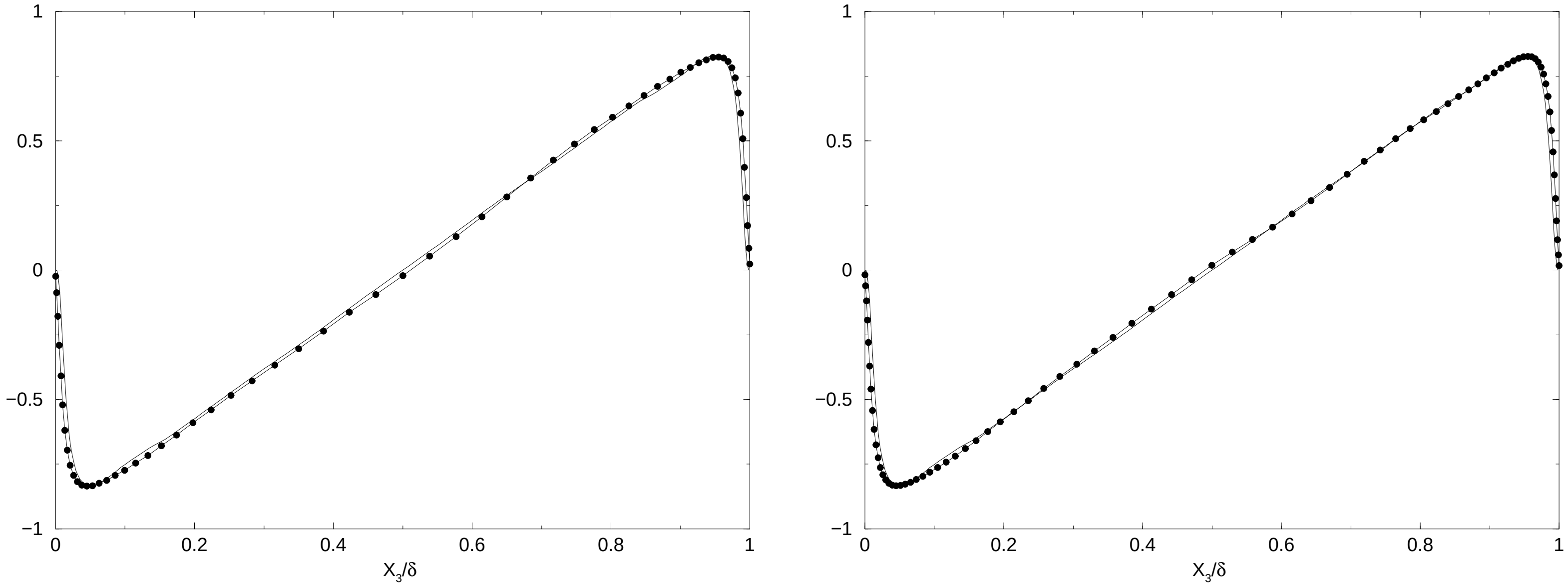

(a) coarse mesh **(b) medium mesh**

Figure 20: Turbulent shear stress $(<(\tau_{13})_{sgs}> + <(\tau_{13})_{les}>)\,/u_\tau^2$**.**
●: (a) LES 1; (b) LES 2; —: DNS. $R_\tau = 395$**.**

- **Evolutions of the total shear stress** $(<(\tau_{13})_{sgs}> + <(\tau_{13})_{les}>)/u_\tau$ **for the coarse and medium meshes. Excellent agreements with DNS data (Moser el al.)**

STREAMWISE TWO-POINTS CORRELATION FUNCTION

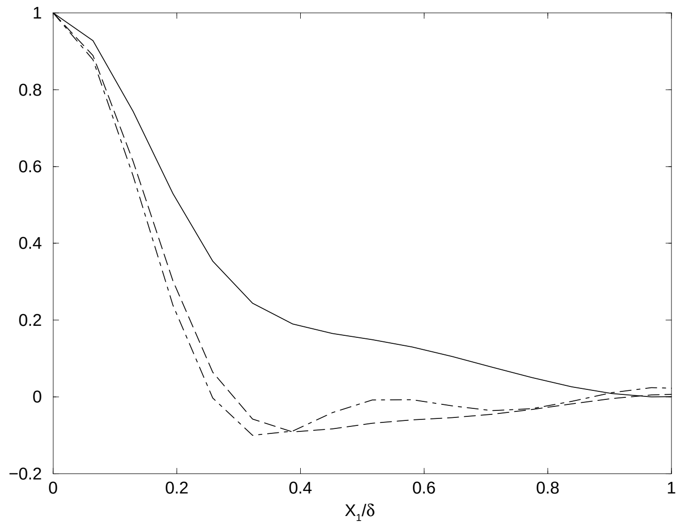

Figure 21: Streamwise two-point correlation tensor. $—\ R_{11}$**;** $-\,-\ R_{22}$**;** $-.-\ R_{33}$**.** $x_3^+ = 390$**,** $x_3 = \delta$**; LES 2.** $R_\tau = 395$**.**

$$R_{ii}(x_1, x_2, x_3) = \frac{\langle u_i'(x_1, x_2, x_3) u_i'(x_1 + r_1, x_2, x_3)\rangle_{LES}}{\langle u_i'^2(x_1, x_2, x_3)\rangle_{LES}} \quad \textbf{(65)}$$

- **Presence of highly elongated eddies in the streamwise direction**

CONTINUOUS HYBRID RANS/LES MODELS (PITM)

- **Injection induceed flows**
  - **Periodicity conditions in the streamwise and spanwise directions**
  - **No slip condition for the upper surface**
  - **Injection condition for the lower surface**
    - **Rate of modeled turbulence injected through the surface** $\sigma_s = \left(\langle u'_2 u'_2 \rangle / u_s^2\right)^{1/2}$
    - **Forcing with a Gaussian velocity distribution in time on the lower surface**
  - **Numerical predictions performed on different grids:** $400 \times 32 \times 80$; $400 \times 44 \times 80$
  - **Influence of the grids in the spanwise direction: tridimensional vorticity effects**

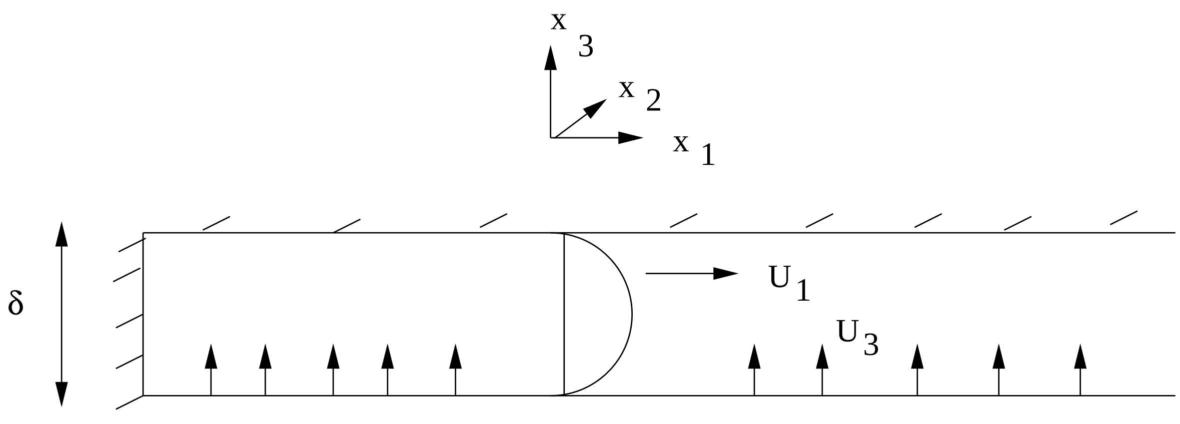

Figure 22: Schematic of channel flow with fluid injection.

INSTANTANEOUS FLOWFIELD STRUCTURES $\delta = 10$ mm.

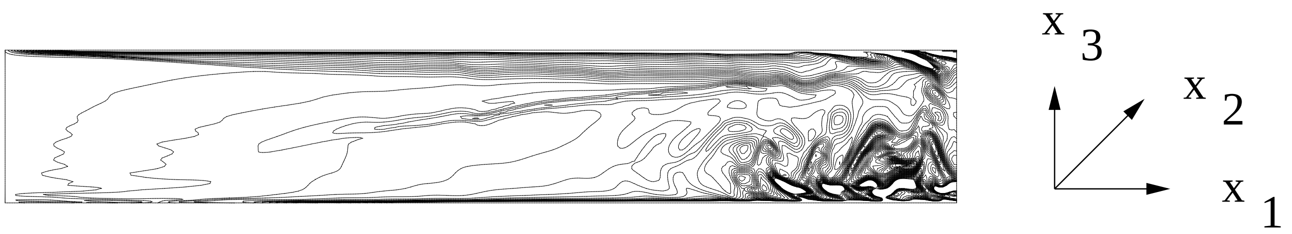

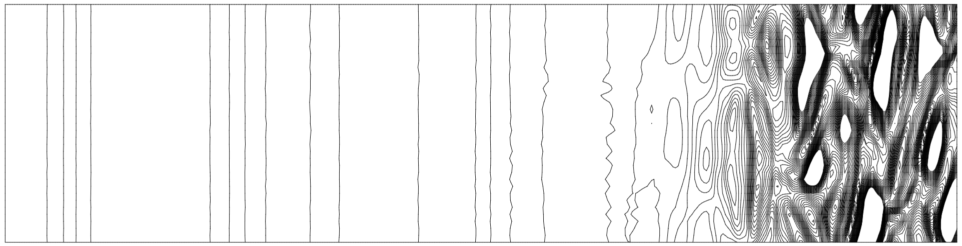

(b)

Figure 23 : Snapshots of spanwise instantaneous filtered vorticity

- **(a) in the (x_1, x_3) plane, $x_2/\delta = 1$. Evolving flow laminar-turbulent regime.**
- **(b) in the (x_1, x_2) plane, $x_3/\delta \approx 0$. Presence of roll-up vortex structures.**

ONERA

STREAMWISE TURBULENT STRESSES $\delta = 10$ mm.

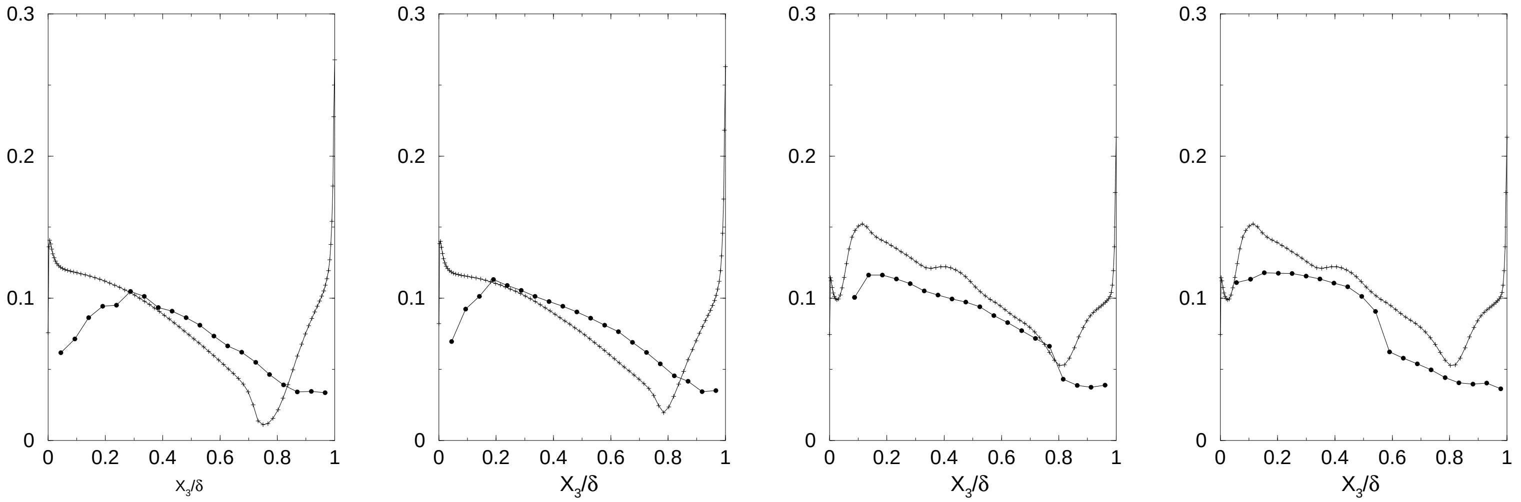

(a) (b) (c) (d)

Figure 25: Streamwise turbulent stresses $< (\tau_{11})^{\frac{1}{2}} > /u_m$ in different cross sections (a) $x_1 = 40$ cm; (b) 45 cm; (c) 50 cm; (d) 57 cm. + : LES ; ●: experimental data.

CONCLUSION

- Second order closure modeling, Reynolds Stress Model (RSM)
  - Transport equations for the Reynolds stress tensor τ_{ij} and for the dissipation-rate ϵ
- Modeling of internal and external flows encountered in aeronautics and space
- Transposition of RSM modeling to hybrid RANS/LES model that allows to obtain a Partial Integrated Transport Model (PITM) for LES on coarse grids
- Future work : modeling and applications
  - Hybrid RANS/LES formulation independent of the wall distance, and of the normal to the wall direction for simulating flows in complex geometries
- The PITM model can be implemented in numerical code using RANS approches with appropriate numerical schemes

References

[1] B. Chaouat. Simulations of channel flows with effects of spanwise rotation or wall injection using a Reynolds stress model. *Journal of Fluid Engineering, ASME*, 123:2–10, 2001.

[2] B. Chaouat. Numerical predictions of channel flows with fluid injection using a Reynolds stress model. *Journal of Propulsion and Power*, 18(2):295–303, 2002.

[3] B. Chaouat and R. Schiestel. Reynolds stress transport modelling for steady and unsteady channel flows with wall injection. *Journal of Turbulence*, 3:1–15, 2002.

[4] B. Chaouat. Reynolds stress transport modeling for high-lift airfoil flows. *AIAA Journal*, 44(10):2390–2403, 2006.

[5] B. Chaouat and R. Schiestel. A new partially integrated transport model for subgrid-scale stresses and dissipation rate for turbulent developing flows. *Physics of Fluids*, 17(065106):1–19, 2005.

[6] B. Chaouat and R. Schiestel. From single-scale turbulence models to multiple-scale and subgrid-scale models by Fourier transform. *Theoretical Computational Fluid Dynamics*, 21(3):201–229, 2007.

[7] R. Schiestel. Multiple-time scale modeling of turbulent flows in one point closures. *Physics of Fluids*, 30(3):722–731, 1987.

[8] R. Schiestel and A. Dejoan. Towards a new partially integrated transport model for coarse grid and unsteady turbulent flow simulations. *Theoretical Computational Fluid Dynamics*, 18:443–468, 2005.

[9] S. S. Girimaji, E. Jeong, and R. Srinivasan. Partially averaged Navier-Stokes method for turbulence: Fixed point analysis and comparisons with unsteady partially averaged Navier-Stokes. *Journal of Applied Mechanics, ASME*, 73(3):422–429, 2006.

[10] U. Schumann. Realizability of Reynolds stress turbulence models. *Physics of Fluids*, 20(5):721–725, 1977.

[11] B. E. Launder and N. Shima. Second moment closure for the near wall sublayer: Development and application. *AIAA Journal*, 27(10):1319–1325, 1989.

[12] C. Cambon, L. Jacquin, and J. L. Lubrano. Toward a new Reynolds stress model for rotating turbulent flows. *Physics of Fluids*, 4(4):812–824, 1992.

[13] M. Lesieur and O. Metais. New trends in large-eddy simulations of turbulence. *Ann. Rev Journal of Fluid Mechanics*, 28:45–82, 1996.

[14] E. Lamballais, O. Métais, and M. Lesieur. Spectral-dynamic model for large-eddy simulations of turbulent rotating flow. *Theoretical Computational Fluid Dynamics*, 12:149–177, 1998.

[1] [2] [3] [4] [5] [6] [7]

[8] [9] [10] [11] [12] [13] [14]